

Optical and Mechanical Rheometry of Semiflexible Main-Chain Thermotropic Liquid-Crystalline Polymers with Varying Pendant Groups

Dong-Ok Kim and Chang Dae Han*

Department of Polymer Engineering, The University of Akron, Akron, Ohio 44325-0301

Patrick T. Mather*,†

Materials and Manufacturing Directorate, Air Force Research Laboratory, Wright Patterson AFB, Ohio 45433-7750

Received May 1, 2000

ABSTRACT: A specially designed flow cell was used to investigate birefringence in transient shear flow, $\Delta n^+(\dot{\gamma}, t)$, of three semiflexible main-chain thermotropic liquid-crystalline polymers (TLCPs), poly[(x)-p-phenylene 1,10-decamethylenebis(4-oxybenzoate)] (PxHQ10) with varying pendant side groups ($x =$ oxyethyleneethoxy, *tert*-butyl, or phenylsulfonyl). Also, shear rheometry was used to investigate the growth of shear stress $\sigma^+(\dot{\gamma}, t)$ and first normal stress difference $N_1^+(\dot{\gamma}, t)$ during transient shear flow of the same TLCPs. Upon startup of shear flow, $\Delta n^+(\dot{\gamma}, t)$ initially increases rapidly, follows two minor overshoots, and then levels off to attain a steady-state value Δn in all three TLCPs. The steady-state value of Δn for PSHQ10 (PxHQ10 with $x =$ phenylsulfonyl pendant side group) was found to be greater than that for PEHQ10 (PxHQ10 with $x =$ ethoxy pendant side group) and PTHQ10 (PxHQ10 with $x =$ *tert*-butyl pendant side group). This behavior is strongly correlated to the large van der Waals volume of phenylsulfonyl pendant side groups in PSHQ10 compared to that of ethoxy pendant side groups in PEHQ10 and *tert*-butyl pendant side groups in PTHQ10. It is also observed that $N_1^+(\dot{\gamma}, t)$ exhibits a very large overshoot followed by an *oscillatory* decay to attain a steady-state value N_1 , while $\sigma^+(\dot{\gamma}, t)$ shows a very large overshoot followed by a rapid *monotonic* decrease to attain a steady-state value, σ . The peak values of $N_1^+(\dot{\gamma}, t)$ and $\sigma^+(\dot{\gamma}, t)$ for PSHQ10 were found to be 3–4 times greater than those for both PEHQ10 and PTHQ10, which we again attribute to the *bulky* phenylsulfonyl pendant side groups in PSHQ10. Only *positive* values of $N_1^+(\dot{\gamma}, t)$ and N_1 were observed over the entire range of shear rates investigated. Variations of the ratio $N_1^+(\dot{\gamma}, t)/\sigma^+(\dot{\gamma}, t)$ with shear strain ($\dot{\gamma}t$) were found to be very similar to variations of $\Delta n^+(\dot{\gamma}, t)$ with $\dot{\gamma}t$ for all three TLCPs investigated, except for that the ratio $N_1^+(\dot{\gamma}, t)/\sigma^+(\dot{\gamma}, t)$ reached a steady state sooner than $\Delta n^+(\dot{\gamma}, t)$. In steady-state shear flow, it is observed that the ratio N_1/σ overlaps Δn over the entire range of temperatures investigated; specifically, both the ratio N_1/σ and Δn remain constant at temperatures far below the clearing temperature (T_{NI}), decrease gradually as the temperature approaches T_{NI} , and drop precipitously to zero value at and near T_{NI} .

1. Introduction

Flow birefringence is a rheoptical technique that offers an alternative and powerful approach to investigate the rheological behavior of polymeric liquids. In the 1960s and 1970s, flow birefringence was used to investigate the rheological behavior of molten *homopolymers* in steady-state shear flow^{1–3} and in the entrance region of a rectangular or slit channel.^{4–6} In recent years birefringence has been used to investigate the rheological behavior of lyotropic solutions^{7–9} as well as to study the dynamics of form birefringence in block copolymer mesophases.¹⁰ However, very few works have specifically addressed the use of birefringence to investigate the rheological behavior of thermotropic liquid-crystalline polymers (TLCPs). A thorough summary of flow birefringence and other optical rheometric methods is available for the interested reader.¹¹ A salient aspect of TLCP rheology is an extreme sensitivity to thermal and deformation histories.^{12–15} Additionally, suitably thin samples and optical methods must be employed to yield birefringence measurements free of multiple-order effects common to polarimetric methods, for example.

As such, the control of initial conditions (i.e., initial morphology) of a specimen is essential to obtain reproducible rheological data that are necessary for the development and testing of a TLCP theory. As demonstrated previously,^{13–16} the initial morphology of a TLCP specimen can be controlled by heating the specimen above its clearing temperature (T_{NI}), shearing in the isotropic phase, and then cooling to a predetermined temperature in the anisotropic state. Such practice is only possible for TLCPs with T_{NI} lower than the thermal degradation temperature. Because no commercial TLCPs meet such a requirement (to our knowledge), the synthesis of model TLCPs is necessary for meaningful investigations of TLCP rheology. These technical challenges may explain the scarcity of flow birefringence data for TLCPs in the literature. However, the additional difficulty of performing elevated temperature rheometry on thin films contributes to the lack of data as well.

It is now well established^{17–21} that attachment of *pendant side groups* to a main-chain TLCP, as an alternative to increasing the spacer length, is very effective in lowering T_{NI} and suppressing crystallization. It can then be reasonably postulated that the size (or bulkiness) of pendant side groups should affect the molecular orientation and rheological behavior of TL-

† Current address: Chemical Engineering Department and Institute of Materials Science, University of Connecticut, Storrs, CT 06269.

Table 1. Summary of the Chemical Structure and van der Waals Volume of Pendant Side Groups, Intrinsic Viscosity, Glass Transition Temperature, and Nematic–Isotropic Transition of the TLCPs Investigated in This Study

sample code	Pendant Side group	van der Waals volume of pendant side group (nm ³)	[η] (dL/g) ^a	T _g (°C)	T _{Nl} (°C)
PEHQ10	OC ₂ H ₅	54.0 × 10 ⁻³	1.393	51	239
PTHQ10	C(CH ₃) ₃	82.7 × 10 ⁻³	0.771	67	193
PSHQ10	SO ₂ - 	121.0 × 10 ⁻³	0.667	84	179

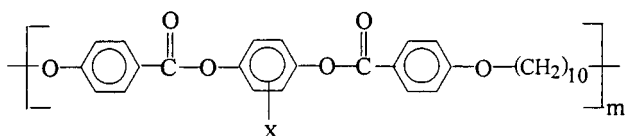
^a Measured at 23 °C on 1,1,2,2-tetrachloroethane.

CPs. Very recently, Kim and Han²² synthesized a series of semiflexible main-chain TLCPs with varying sizes of pendant side groups in order to investigate the effect of the size of pendant side groups on phase transitions and rheological behavior.

As part of our continuing effort toward a better understanding of the rheology of TLCPs, we investigated in this study the birefringence of semiflexible main-chain TLCPs with varying sizes of pendant side groups in both the transient and steady-state shear flows using a specially designed flow cell. We also investigated the growth of shear stress $\sigma^+(\dot{\gamma}, t)$ and first normal stress difference $N_1^+(\dot{\gamma}, t)$ during transient shear flow of the same TLCPs using shear rheometry for comparison. We examined the results of birefringence and shear rheometry in both transient and steady-state shear flows and compared the temperature dependence of birefringence and the ratio $N_1^+(\dot{\gamma}, t)/\sigma^+(\dot{\gamma}, t)$ over a wide range of temperatures covering the nematic, biphasic, and isotropic regions. In this paper we report the highlights of our findings.

2. Experimental Section

2.1. Materials. We synthesized three semiflexible main-chain TLCPs, poly[(x)-p-phenylene 1,10-decamethylenebis(4-oxybenzoate)] (PxHQ10) with chemical structure



Below, PxHQ10 with $x = \text{OC}_2\text{H}_5$ will be referred to as PEHQ10, PxHQ10 with $x = \text{C}(\text{CH}_3)_3$ will be referred to as PTHQ10, and PxHQ10 with $x = \text{SO}_2\text{-Ph}$ will be referred to as PSHQ10. The readers are referred to previous papers^{17–21} for the details of the synthesis procedures for the PxHQ10 employed in this study. The sample codes and the intrinsic viscosities determined using an Ubbelohde viscometer of the polymers synthesized are given in Table 1. An objective of this paper is to show the effect of the size of pendant side groups on flow birefringence and shear flow behavior of the TLCPs synthesized; therefore, we have calculated the van der Waals volume, using the Cerius² program (Molecular Simulations Inc.), of the three pendant side groups. The results are also given in Table 1. To facilitate our discussion later, in Table 1 are also summarized thermal transition temperatures, determined via differential scanning calorimetry, of the three TLCPs synthesized. We note that PEHQ10 undergoes smectic-to-nematic (S–N) transition at 148 °C and nematic-to-isotropic (N–I) transition at 239 °C, while both PTHQ10 and PSHQ10 undergo only N–I transition: PTHQ10 at 193 °C and PSHQ10 at 179 °C. Additionally, the three polymers exhibit glass transition temperatures of 51, 67, and 84 °C for PEHQ10, PTHQ10, and PSHQ10, respectively.

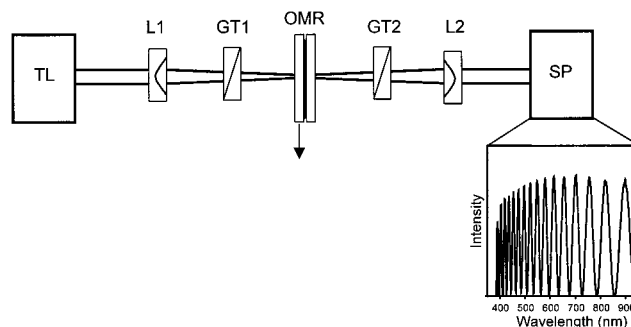


Figure 1. Schematic of the optical train used to measure flow-induced birefringence of thin, heated polymer films. White Light (TL) is focused on the sample shearing plane (OMR), using a lens (L1), and polarized (GT1) at an angle 45° from the flow axis. Light then passes through an analyzer (GT2) parallel with the polarizer and collected with a lens (L2) to a spectrometer (SP).

2.2. Sample Preparation. Specimens with a thickness of 0.5 mm were prepared by solvent casting from dichloromethane with 0.1 wt % antioxidant (Irganox 1010, Ciba-Geigy Group) and then slowly evaporating the majority of the solvent first at room temperature for 1 week and then at 10 °C below the glass transition temperature (T_g) for 3 days in a vacuum oven to remove any residual solvent. Further, specimens were dried in a vacuum oven at $T_g + 10$ °C for 2 h.

2.3. Flow Birefringence Measurement. To monitor the evolution of flow-induced birefringence of the TLCPs in this study, we employed a custom optical microrheometer previously described in some detail.^{23,24} Shearing flow is imposed between parallel quartz plates at elevated temperature with provision for shear stress measurement, all controlled by customized software written in the C++ programming language. Sample thicknesses of 50.8 μm are used in all cases, unless otherwise noted. Such thicknesses are achieved using careful planarizing and offsetting of the quartz plates with a kinematic mount, followed by sample compression and annealing under a normal load of 500 g force. Previous experiments on TLCP rheoptics²⁵ have revealed large birefringences, $\Delta n \sim 0.1$, leading to expected retardances in the range $\Delta n h \sim 5000$ nm for the thicknesses of our samples. Therefore, we have adopted a spectrographic birefringence technique.^{26,27} To the best of our knowledge, spectrographic birefringence has not been previously applied to in-situ measurements on flowing TLCPs, despite the power of this method. The optical train for our spectrographic birefringence setup is shown schematically in Figure 1. White light from a tungsten lamp (LS-1, TL) is coupled to a fiber-optic cable, and the light beam is then focused upon the sample-shearing plane (OMR) using a 10 cm working distance objective lens (L1) while passing through a Glan-Thompson polarizer (GT1) for linear polarization oriented 45° away from the flow axis. After passing through the shear cell, the light, whose polarization state and spectral content have been modified by the birefringent sample, then passes through a second Glan-Thompson polarizer (analyzer, GT2) oriented parallel with the incident polarizer and then collected using a receiving objective lens (L2) mated with a fiber-optic cable. The light spectrum thus received is analyzed using an Ocean Optics spectrometer (S2000, SP) and OOIBase software. The raw intensity spectra were normalized using the following formula

$$T(\lambda) = (I(\lambda) - I_d(\lambda))/(I_0(\lambda) - I_d(\lambda)) \quad (1)$$

where $I_0(\lambda)$ is the spectrum of the unoriented polymer in the isotropic phase and $I_d(\lambda)$ is the dark spectrum obtained when the light source is blocked.

For parallel polarizers, the measured transmission spectra are given by the relation²⁸

$$T(\lambda) = A_s \cos^2\left(\frac{\pi \Delta n h}{\lambda}\right) \quad (2)$$

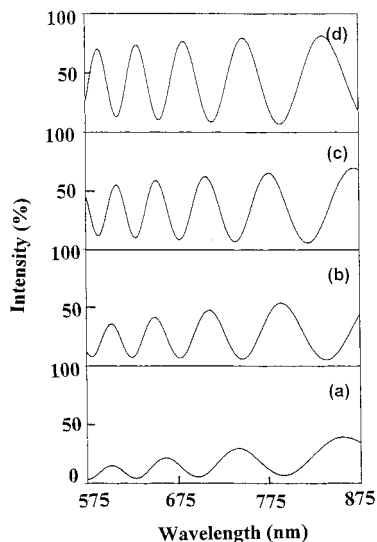


Figure 2. Transmission spectra for PSHQ10 during shear start-up with measurements taken at (a) 9, (b) 18, (c) 72, and (d) 216 strain units, with $\dot{\gamma} = 0.3 \text{ s}^{-1}$ and at $T_{\text{NI}} - 30 \text{ }^\circ\text{C}$. For each trace, the intensity data are expressed as a percentage of the light transmitted by the polymer in the isotropic phase. Incident light is polarized at an angle 45° to the flow axis and the analyzer is parallel to the polarizer.

We have previously described a new approach to the analysis of data using eq 2, in which a selected spectral window of data, namely $575 < \lambda < 775 \text{ nm}$, is analyzed using a fast Fourier transform (FFT) method.²⁹ It is noted that, over this relatively narrow range wavelength, dispersion of birefringence is minimal, as indicated by a narrow FFT power spectrum. Calibration of both the spectrometer and numerical processing was performed using multiorder retarders with known retardance (Melles Griot). The square root of the peak magnitude is equivalent to the amplitude of the spectral oscillations, with values ranging from 0 to 1, and is referred to as the spectrum amplitude, $A_s^+(t, \dot{\gamma})$, below.

2.4. Rheological Measurements. A Rheometrics mechanical spectrometer (RMS model 800) with a cone-and-plate (8 mm diameter plate, 0.1 rad cone angle) fixture was used to measure (i) shear stress growth ($\sigma^+(t, \dot{\gamma})$) and first normal stress difference growth ($N_1^+(t, \dot{\gamma})$) during startup shear flow for various shear rates ($\dot{\gamma}$) and (ii) shear stress (σ) and first normal stress difference (N_1) for various $\dot{\gamma}$ in steady-state shear flow. To erase previous thermal history, before beginning rheological measurements a solvent-cast specimen was first heated to $T_{\text{NI}} + 10 \text{ }^\circ\text{C}$ in the isotropic state, held there for about 5 min while being sheared at a rate of 0.5 s^{-1} , and then cooled to a predetermined temperature in the nematic region. All experiments were conducted under a nitrogen atmosphere in order to preclude oxidative degradation of the specimen. The temperature control was satisfactory to within $\pm 1 \text{ }^\circ\text{C}$.

3. Results and Discussion

3.1. Birefringence in Startup of Shear Flow in the Nematic Region. When shear flow is applied to the samples, dramatic changes in the polarized visible transmission spectrum occur, as shown in Figure 2 for PSHQ10 sheared at $\dot{\gamma} = 0.3 \text{ s}^{-1}$. It can be seen that as shear strain is accumulated, the material begins to transmit light increasingly, as indicated by an increase in the overall intensity magnitude. Meanwhile, the birefringence grows dramatically, as indicated by the increased number of intensity oscillations visible over a given wavelength range. Analysis of these spectra, and spectra for polymers of varying pendant group size, reveal that the transmitted intensity and birefringence follow dynamics distinct from one another, as we now detail.

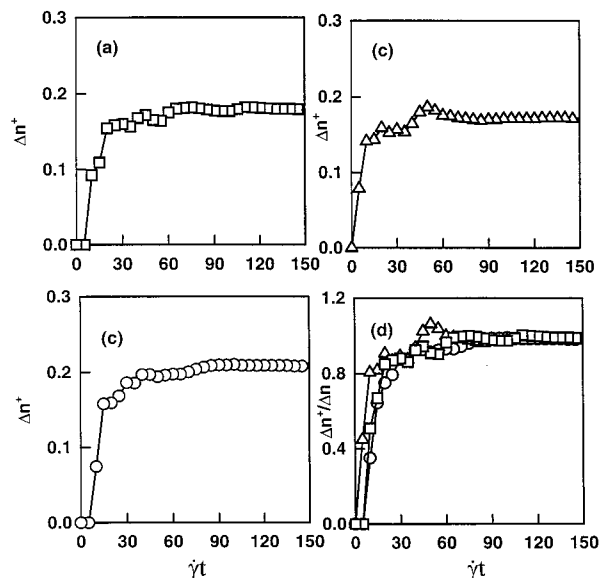


Figure 3. (a) Variations of $\Delta n^+(t, \dot{\gamma})$ with $\dot{\gamma}t$ for PEHQ10, (b) variations $\Delta n^+(t, \dot{\gamma})$ with $\dot{\gamma}t$ for PTHQ10, (c) variations of $\Delta n^+(t, \dot{\gamma})$ with $\dot{\gamma}t$ for PSHQ10, and (d) variations of normalized birefringence $\Delta n^+(t, \dot{\gamma})/\Delta n$ with $\dot{\gamma}t$ for (□) PEHQ10, (△) PTHQ10, and (○) PSHQ10 at $\dot{\gamma} = 0.3 \text{ s}^{-1}$ and $T_{\text{NI}} - 30 \text{ }^\circ\text{C}$ upon startup of shear flow, where Δn is the steady-state value of birefringence. Table 1 summarizes values of T_{NI} of each polymer.

Figure 3 shows the birefringence growth $\Delta n^+(t, \dot{\gamma})$ for (a) PEHQ10, (b) PTHQ10, (c) PSHQ10, and (d) normalized birefringence growth, $\Delta n^+(t, \dot{\gamma})/\Delta n$, in startup of shear flow at $T_{\text{NI}} - 30 \text{ }^\circ\text{C}$ for PEHQ10, PTHQ10, and PSHQ10 at $\dot{\gamma} = 0.3 \text{ s}^{-1}$ until reaching a steady state. In Figure 3, Δn denotes the steady-state birefringence and $\dot{\gamma}t$ denotes strain with t being the duration of shear flow applied. Here, we observe that initially $\Delta n^+(t, \dot{\gamma})$ increases rapidly, with small local maxima, and then levels off to attain a steady-state value Δn . Interestingly, we observe in Figure 3 that Δn for PSHQ10 is higher than that of PEHQ10 and PTHQ10. This is correlated with the presence of bulky phenylsulfonyl pendant side groups in PSHQ10 (see Table 1 for the van der Waals volume of the three pendant side groups). However, plots of $\Delta n^+(t, \dot{\gamma})/\Delta n$ versus $\dot{\gamma}t$ given in Figure 3d show little difference among the three TLCs investigated, except that upon startup of shear flow the growth of birefringence in PTHQ10 is faster than in the other two TLCs.

In view of the fact that flow birefringence describes the extent of orientation of polymer chains during flow, it is expected that the molecular weight of a polymer should play an important role in determining both transient and steady-state flow birefringence responses, primarily through its effect on the viscosity magnitude.³⁰ Therefore, the fact that the samples under investigation feature differing molecular weight (see Table 1 for intrinsic viscosity data) has potential bearing on our observations. Temperature should also play an important role in determining the values of $\Delta n^+(t, \dot{\gamma})$ and Δn , in relation to both the magnitude of the viscosity and the strength of local nematic ordering. To minimize variations due both to molecular weight and temperature (local nematic ordering), thus allowing *material* comparisons, we have chosen to examine responses at fixed temperatures below the clearing transition, $T = T_{\text{NI}} - 30 \text{ }^\circ\text{C}$. The rationale behind this approach lies in the fact that T_{NI} decreases with decreasing molecular weight values lower than a certain critical value (say

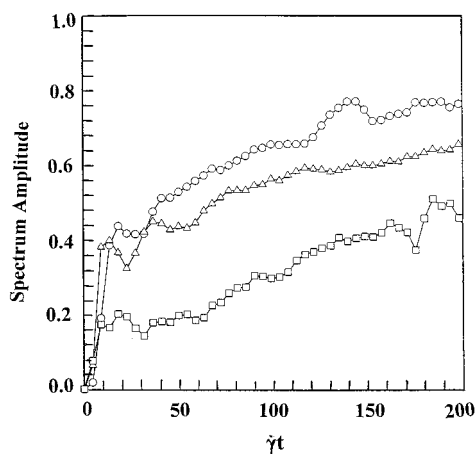


Figure 4. Variations of normalized spectrum amplitude $A_s^+(t, \dot{\gamma})$, computed from the amplitude of the FFT power spectrum of the transmitted intensity, with $\dot{\gamma}t$ upon startup of shear flow for (□) PEHQ10, (△) PTHQ10, and (○) PSHQ10 at $\dot{\gamma} = 0.3 \text{ s}^{-1}$ and $T_{\text{NI}} = 30 \text{ }^\circ\text{C}$.

ca. 30 000 g/mol).^{30–35} Therefore, concerning phase behavior and rheoptical changes associated with the clearing transition, the choice of T_{NI} as a reference temperature minimizes, if not eliminating completely, the effect of molecular weight on $\Delta n^+(t, \dot{\gamma})$ and Δn . More specifically, it has been amply demonstrated in the literature^{21,36–38} that the viscosity of TLCPs in the nematic state first decreases, going through a minimum, and then increases, going through a maximum at T_{NI} , finally decreasing again as the temperature is increased from the nematic state to the isotropic state. Therefore, a comparison of molecular orientation, via birefringence, of TLCPs in the nematic state at temperatures having the same distance below the respective T_{NI} values would seem reasonable. In fact, earlier Chang and Han³⁹ successfully used the same approach to compare the melt viscosities of a homologous series of semiflexible main-chain TLCPs.

Figure 4 describes the evolution of the spectrum amplitude $A_s^+(t, \dot{\gamma})$, upon startup of shear flow at $T_{\text{NI}} = 30 \text{ }^\circ\text{C}$ for PEHQ10, PTHQ10, and PSHQ10 at $\dot{\gamma} = 0.3 \text{ s}^{-1}$. Note that $A_s^+(t, \dot{\gamma})$ data reflect the amplitude in spectral transmission oscillations (eq 2) relative to the case of a perfect optical retarder, for which A_s is unity, so that fractional values indicate nonideal retardation of the incoming polarized light. Several features observed on inspecting the plots are worth noting. First, all three samples show initially rapid increases in spectrum amplitude, occurring within the first 10 strain units, that give way to very slow growths which are still incomplete after 200 strain units. Second, PTHQ10 and PSHQ10 show quantitatively similar behavior for $A_s^+(t, \dot{\gamma})$ that leads asymptotically to $A_s = 0.6\text{--}0.7$, while distinctly lower asymptotic values are observed for PEHQ10 when exposed to the same shearing conditions.

Here, we interpret the spectrum amplitude data, upon startup of shear flow, as a manifestation of flow-induced textural coarsening, with large amplitudes indicating less scattering of light away from our detector by nematic disclinations (i.e., a coarser texture). A second interpretation of these observations is that fractional A_s data may arise from polarization state mixing;²⁶ however, we have found trends similar to those in Figure 4 using a different optical technique. In particular, we have compared $A_s^+(t, \dot{\gamma})$ data with the growth in unpolarized light transmission (“transmission”) as mea-

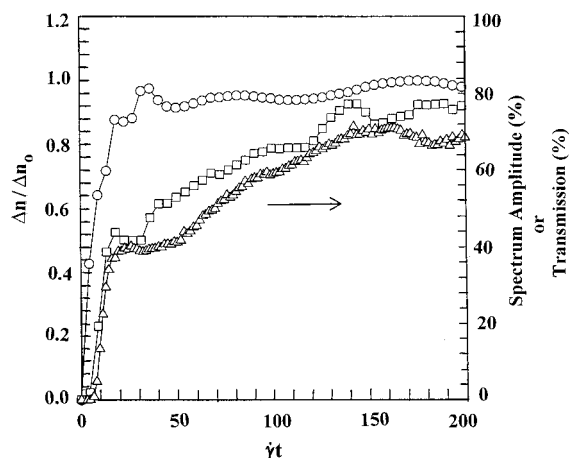


Figure 5. Variations of $\Delta n^+(t, \dot{\gamma})$ (○), $A_s^+(t, \dot{\gamma})$ (□), and transmission (△), with $\dot{\gamma}t$ for PSHQ10 at $\dot{\gamma} = 0.3 \text{ s}^{-1}$ and $T_{\text{NI}} = 30 \text{ }^\circ\text{C}$.

sured at a wavelength of 700 nm with no analyzer and relative to the intensity transmitted by an isotropic sample. In Figure 5, it is clearly seen that transmission data measured in this way closely track spectrum amplitude observations while, conversely, show an evolution in time somewhat independent of the growth in birefringence. Thus, it appears that scattering of light by the defect texture plays a dominant role in determining the observed A_s data and that birefringence growth and defect texture coarsening ($A_s^+(t, \dot{\gamma})$) follow different kinetics.

As shown in Table 1, among the three TLCPs, PEHQ10 has the highest intrinsic viscosity and thus the highest molecular weight. Therefore, despite having the smallest pendant group among the three TLCPs, PEHQ10 features the smallest level of flow-induced textural coarsening upon startup of shear flow owing to its high molecular weight. However, Kim and Han²² have shown before, and we will show below, that PSHQ10 features a higher steady-state viscosity than PEHQ10, despite having a lower intrinsic viscosity. It is then apparent that the bulkiness of pendant side group effectively increases melt viscosity (at fixed $T_{\text{NI}} - T$) in the nematic phase as T_{NI} dramatically decreases while T_g slightly increases with increasing volume of pendant side group.

Indeed, the extent of textural coarsening indicated by $A_s^+(t, \dot{\gamma})$ measurements is most directly correlated to $\Delta T = T - T_g$ and the magnitude of shear viscosity, which we were unable to vary independently from ($T_{\text{NI}} - T$) for reasons just explained. In this way, those TLCPs with larger pendant side groups feature expedited coarsening due, apparently, to a larger shear viscosity. This result suggests the utility of comparable experiments performed under conditions of controlled shear stress. To date, however, the development of a controlled stress optical rheometer for TLCPs has not been achieved.

Figure 6 gives plots of Δn versus $\dot{\gamma}$ in steady-state shear flow of the three TLCPs investigated at $T_{\text{NI}} = 30 \text{ }^\circ\text{C}$. In Figure 6 we observe that in the nematic region Δn of PEHQ10 and PTHQ10 is virtually independent of $\dot{\gamma}$ over the entire range of shear rates tested, while Δn of PSHQ10 increases slowly with $\dot{\gamma}$ until reaching $\dot{\gamma} \approx 1.0 \text{ s}^{-1}$ and then decreases sharply followed by an oscillatory behavior. During the experiment we detected evidence of flow instability occurring in PSHQ10 at $\dot{\gamma}$

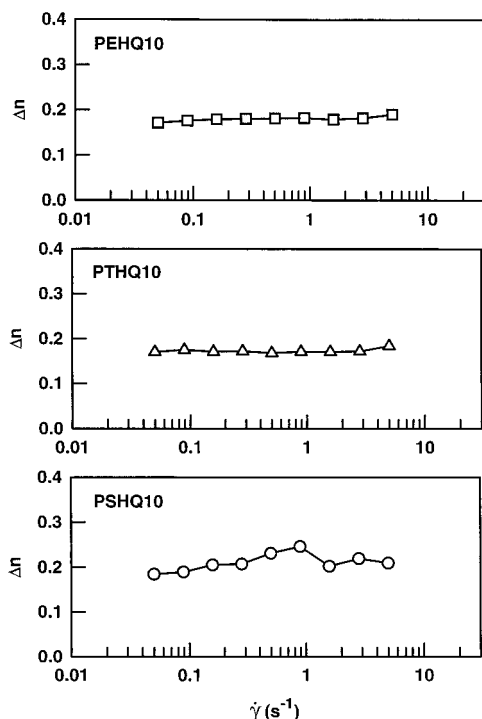


Figure 6. Plots of Δn versus $\dot{\gamma}$ in steady-state shear flow for (□) PEHQ10, (Δ) PTHQ10, and (○) PSHQ10 at $T_{NI} = 30$ °C.

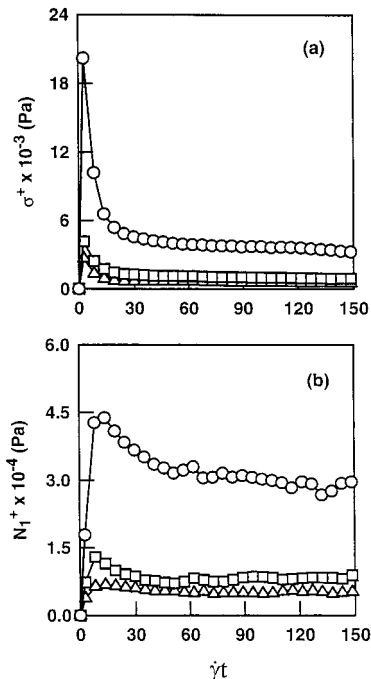


Figure 7. (a) Variations of $\sigma^+(t, \dot{\gamma})$ with $\dot{\gamma}t$ and (b) variations of $N_1^+(t, \dot{\gamma})$ with $\dot{\gamma}t$ upon startup of shear flow at $\dot{\gamma} = 0.3$ s⁻¹ and $T_{NI} = 30$ °C for (□) PEHQ10, (Δ) PTHQ10, and (○) PSHQ10.

≈ 1.0 s⁻¹ and higher. Earlier Ugaz and Burghardt⁴⁰ reported that steady-state level of molecular orientation in a TLCP (PSHQ6-12) was fairly insensitive to shear rate over the range of shear rates tested.

3.2. Growth of Shear Stress and Normal Stress Difference upon Startup of Shear Flow in the Nematic Region. Figure 7 compares shear stress buildup $\sigma^+(t, \dot{\gamma})$ and first normal stress difference buildup $N_1^+(t, \dot{\gamma})$ upon startup of shear flow at $T_{NI} = 30$ °C for the PEHQ10, PTHQ10, and PSHQ10 at $\dot{\gamma} = 0.3$ s⁻¹. In

Figure 7 we observe that (i) the peak value of $N_1^+(t, \dot{\gamma})$ is 3–4 times greater than that of $\sigma^+(t, \dot{\gamma})$, (ii) $N_1^+(t, \dot{\gamma})$ exhibits multiple peaks with oscillatory decay with increasing $\dot{\gamma}t$, while $\sigma^+(t, \dot{\gamma})$ decays monotonically with increasing $\dot{\gamma}t$, approaching a steady state, and (iii) only positive values of $N_1^+(t, \dot{\gamma})$ are observed over the entire range of $\dot{\gamma}t$ tested, which is consistent with the previous studies^{14,15,30,38,39,41–43} on TLCPs. It is worth noting in Figure 7 that the peak values of $\sigma^+(t, \dot{\gamma})$ and $N_1^+(t, \dot{\gamma})$ for PSHQ10 are 3–4 times greater than those for PEHQ10 and PTHQ10. This is attributable to the presence of phenylsulfonyl pendant side groups in PSHQ10, which are bulkier than ethoxy pendant side groups in PEHQ10 and *tert*-butyl pendant side groups in PTHQ10 (see Table 1 for van der Waals volume of the three different pendant side groups). Specifically, the steady-state viscosity of PSHQ10 is higher than that of PEHQ10, despite having an apparently lower molecular weight.

It should be mentioned at this juncture that earlier Marrucci and Maffettone⁴⁴ predicted multiple overshoots in $N_1^+(t, \dot{\gamma})$ during transient shear flow of nematics with the aid of the Maier–Saupe potential⁴⁵ that may be valid for small-molecule liquid crystals. Since the Marrucci–Maffettone analysis is based on the Doi theory⁴⁶ predicting director “tumbling”, we must examine whether mild oscillations in $N_1^+(t, \dot{\gamma})$ observed in Figure 7 may signify the presence of director “tumbling”. According to Marrucci and Maffettone⁴⁷ and Larson,⁴⁸ who implicated director “tumbling” in the phenomenon of negative N_1 , we conclude from Figure 7 that all three polymers investigated in this study may not be of “tumbling” type, because no negative N_1 has been observed.

Since Figure 7 gives experimental data at one temperature, $T_{NI} = 30$ °C (i.e., 209 °C for PEHQ10, 163 °C for PTHQ10, and 149 °C for PSHQ10), and at one shear rate, $\dot{\gamma} = 0.3$ s⁻¹, let us examine the previous experimental data for PSHQ10 investigated at varying temperatures and shear rates.¹⁴ Specifically, Figures 9–11 of ref 14 show that $N_1^+(t, \dot{\gamma})$ of PSHQ10 exhibits a single overshoot at all three temperatures tested, 130, 140, and 150 °C, for $\dot{\gamma} = 0.107$ s⁻¹ but multiple overshoots with oscillatory decay at 130 and 140 °C for $\dot{\gamma} = 0.536$ and 1.07 s⁻¹ while a single overshoot at 150 °C for $\dot{\gamma} = 0.536$ and 1.07 s⁻¹. It is clear from the above observations that multiple overshoots in $N_1^+(t, \dot{\gamma})$ for PSHQ10 appear as the shear rate is increased above a certain critical value and as the temperature is decreased below a certain critical value. It is significant to observe in Figure 13 of ref 14, however, that PSHQ10 exhibits only positive values of N_1 over the entire range of $\dot{\gamma}$ (0.109–2.69 s⁻¹) tested at 130, 140, and 150 °C. A serious question then may be raised: Can the multiple overshoots in $N_1^+(t, \dot{\gamma})$ observed for PSHQ10 be regarded as signifying the presence of director “tumbling” in the absence of negative N_1 ? If not, what might be the origin(s) of multiple overshoots in $N_1^+(t, \dot{\gamma})$ observed for PSHQ10? If the multiple overshoots in $N_1^+(t, \dot{\gamma})$ observed for PSHQ10 are not related to director “tumbling” in the absence of negative N_1 , we must then seek for other explanations on the experimental observations. From this perspective, we note that the mild oscillations in $N_1^+(t, \dot{\gamma})$ observed in Figure 7, and the pronounced oscillations in $N_1^+(t, \dot{\gamma})$ reported in ref 14 have little to do with the multiple overshoots in $N_1^+(t, \dot{\gamma})$ predicted by Marrucci and Maffettone.⁴⁴ This subject remains to be addressed in future study.

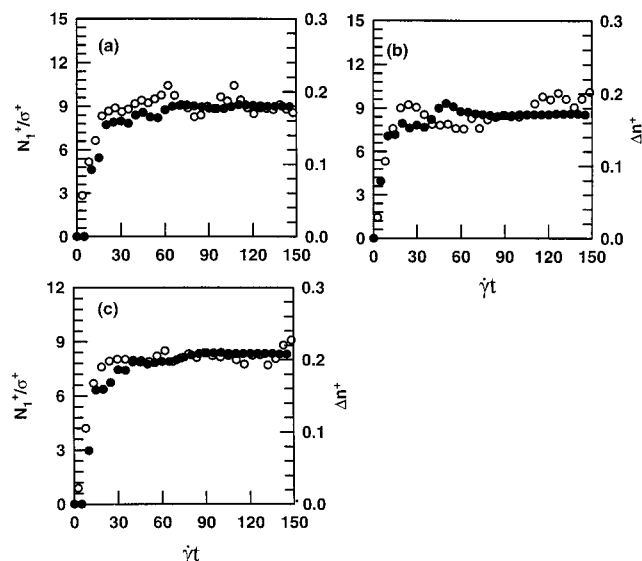


Figure 8. Plots of $N_1^+(t, \dot{\gamma})/\sigma^+(t, \dot{\gamma})$ versus $\dot{\gamma}t$ (○) and $\Delta n^+(t, \dot{\gamma})$ versus $\dot{\gamma}t$ (●) upon startup of shear flow at $\dot{\gamma} = 0.3 \text{ s}^{-1}$ and $T_{\text{NI}} - 30 \text{ }^\circ\text{C}$ for (a) PEHQ10, (b) PTHQ10, and (c) PSHQ10.

Notice in Figure 7 that all three polymers exhibit a single overshoot in $\sigma^+(t, \dot{\gamma})$ at $T_{\text{NI}} - 30 \text{ }^\circ\text{C}$ (i.e., $209 \text{ }^\circ\text{C}$ for PEHQ10, $163 \text{ }^\circ\text{C}$ for PTHQ10, and $149 \text{ }^\circ\text{C}$ for PSHQ10) for $\dot{\gamma} = 0.3 \text{ s}^{-1}$. At present we ascribe such an experimental observation to the tendency toward a transformation from polydomain texture into monodomain texture. This viewpoint seems to be supported by our most recent rheoptical study combined with in-situ polarizing optical microscopy,²⁹ showing an evolution of domain texture upon shear startup of PSHQ10 while exhibiting a single overshoot in $\sigma^+(t, \dot{\gamma})$. Let us now examine Figures 6–8 of ref 14, showing that $\sigma^+(t, \dot{\gamma})$ of PSHQ10 exhibits a single overshoot at 140 and 150 $^\circ\text{C}$ for all three shear rates tested, $\dot{\gamma} = 0.107, 0.536,$ and 1.07 s^{-1} but at 130 $^\circ\text{C}$ a mild second overshoot for $\dot{\gamma} = 0.536$ and 1.07 s^{-1} while a single overshoot for $\dot{\gamma} = 0.107 \text{ s}^{-1}$. In other words, $\sigma^+(t, \dot{\gamma})$ tends to exhibit multiple overshoots as the shear rate is *increased* above a certain critical value and as the temperature is *decreased* below a certain critical value, very similar to the observation made above for multiple overshoots in $N_1^+(t, \dot{\gamma})$ with reference to Figures 9–11 of ref 14.

Earlier, Ugaz and Burghardt⁴⁰ conducted X-ray scattering experiments on a semiflexible main-chain thermotropic random copolymer (PSHQ6-12) with phenyl-sulfonyl pendant side groups and determined the degree of molecular orientation (S) using high-flux wide-angle X-ray scattering. They observed that, upon shear startup, S increased monotonically to a steady-state value. On the basis of their X-ray scattering experiments and the earlier experimental results of Chang and Han,⁴² who reported a single, large overshoot in $\sigma^+(t, \dot{\gamma})$ during transient shear flow, Ugaz and Burghardt⁴⁰ concluded that PSHQ6-12 was of “flow-aligning” type. It should be mentioned that PSHQ6-12 exhibits only *positive* values of N_1 .⁴²

3.3. Correlation between Birefringence and Shear Rheometry. In the course of our studies, we have often seen striking similarity between trends in birefringence and the ratio of first normal stress difference to shear stress. In particular, Figure 8 gives plots of $N_1^+(t, \dot{\gamma})/\sigma^+(t, \dot{\gamma})$ versus $\dot{\gamma}t$ (○) and $\Delta n^+(t, \dot{\gamma})$ versus $\dot{\gamma}t$ (●) upon startup of shear flow at $\dot{\gamma} = 0.3 \text{ s}^{-1}$ and $T_{\text{NI}} - 30 \text{ }^\circ\text{C}$ for (a) PEHQ10, (b) PTHQ10, and (c) PSHQ10.

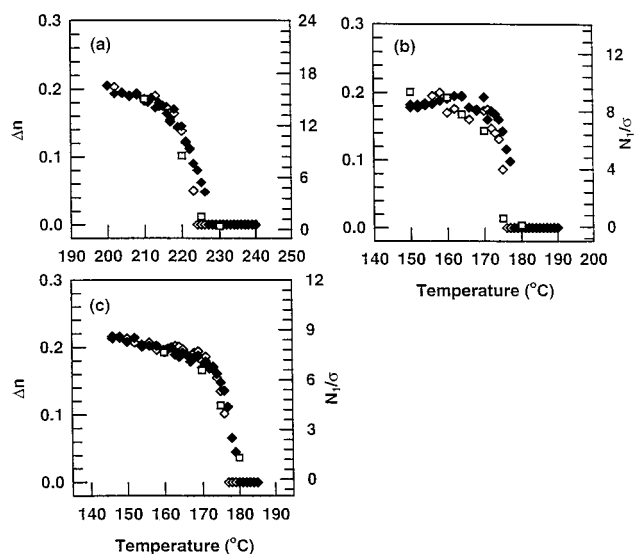


Figure 9. Temperature dependence of steady-state birefringence Δn at $\dot{\gamma} = 0.05 \text{ s}^{-1}$ in the heating (◆) and cooling processes (◇) and temperature dependence of steady-state stress ratio N_1/σ at $\dot{\gamma} = 0.05 \text{ s}^{-1}$ (□) for (a) PEHQ10, (b) PTHQ10, and (c) PSHQ10.

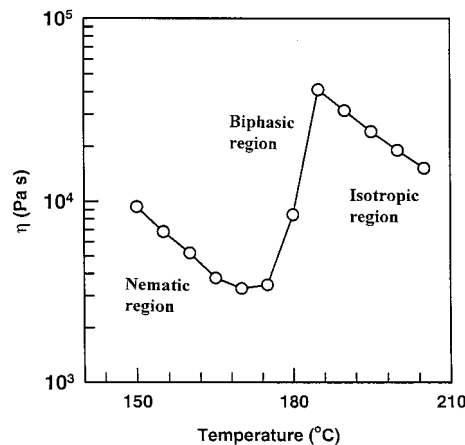


Figure 10. Temperature dependence of steady-state shear viscosity for PSHQ10 at $\dot{\gamma} = 0.3 \text{ s}^{-1}$.

In Figure 8 we observe that plots of $N_1^+(t, \dot{\gamma})/\sigma^+(t, \dot{\gamma})$ versus $\dot{\gamma}t$ overlap reasonably well with plots of $\Delta n^+(t, \dot{\gamma})$ versus $\dot{\gamma}t$ in all three TLCPs investigated, except that the ratio $N_1^+(t, \dot{\gamma})/\sigma^+(t, \dot{\gamma})$ tends to attain a steady state sooner than $\Delta n^+(t, \dot{\gamma})$. No overshoot in the ratio $N_1^+(t, \dot{\gamma})/\sigma^+(t, \dot{\gamma})$ is observed in Figure 8. Using an averaging scheme of Ericksen’s transversely isotropic fluid model,⁴⁹ very recently Burghardt⁵⁰ calculated the ratio N_1/σ and Δn as a function of $\dot{\gamma}$ showing a qualitative agreement with our experimental results given in Figure 8.

Figure 9 gives plots of Δn versus temperature and N_1/σ versus temperature for PEHQ10, PTHQ10, and PSHQ10 for steady shearing at a low shear rate of 0.05 s^{-1} . We observe surprisingly good overlap between Δn and N_1/σ over a wide range of temperatures investigated. To facilitate discussion of these data below, a plot of steady-state shear viscosity η versus temperature is given in Figure 10 for PSHQ10 at temperatures, spanning the nematic, biphasic, and isotropic regions. It should be mentioned that the biphasic region observed in Figure 10 (viscosity increasing with temperature) exists due to the polydisperse nature of the polymer (polydispersity index of about 2.5).³⁰ Moreover, TLCP clearing temperatures depend on molecular weight

below a certain critical value.^{30–35,51,52} Therefore, the temperature (T_{NI}) at which η goes through a maximum in Figure 10 corresponds to the clearing of the highest molecular weight fractions while the minimum (at a lower temperatures) corresponds to the clearing of the lowest molecular weight TLCP chains. If the polymer were monodisperse, the biphasic region in Figure 10 would be extremely narrow.

In light of our understanding gleaned from Figure 10, we now describe the data of Figure 9 in more detail. For temperatures well below T_{NI} we observe only a weak (decreasing) temperature dependence for both Δn and the ratio N_1/σ , while for temperatures approaching T_{NI} , we observe that Δn and N_1/σ begin to decrease gradually as the temperature approaches T_{NI} , i.e., in the biphasic region. At a certain critical temperature close to T_{NI} , Δn and the ratio N_1/σ drop precipitously. The temperature dependence of Δn and the ratio N_1/σ given in Figure 9 can be understood with the aid of Figure 10, showing how η varies with temperature in the nematic, biphasic, and isotropic regions. Particularly noteworthy in Figure 9 is the observation that Δn and the ratio N_1/σ for PEHQ10 and PTHQ10 drop virtually to zero at a temperature 15–18 °C below T_{NI} , while Δn and the ratio N_1/σ for PSHQ10 become virtually zero only at temperatures much closer to T_{NI} . In view of the fact that Δn describes molecular alignment of the polymer in steady-state shear flow, it is clear from Figure 9 that PEHQ10 and PTHQ10 begin to lose molecular alignment at temperatures 15–18 °C below T_{NI} . This suggests two possibilities. First, it is possible that PEHQ10 and PTHQ10 might feature much broader molecular weight distributions than PSHQ10, so that the low-molecular-weight portion of the polymers begin isotropization at temperatures 15–18 °C below T_{NI} . Second, it is possible that the smaller (or less bulky) ethoxy pendant side groups in PEHQ10 and *tert*-butyl pendant side groups in PTHQ10, compared to the bulky phenylsulfonyl pendants in PSHQ10, might destabilize molecular alignment at lower temperatures. We presently prefer the former explanation, but this will be tested in future experiments. Nevertheless, the salient result of Figure 9 is the finding of significant correlation between the *optical* birefringence and the *mechanical* stress ratio N_1/σ , suggesting a new stress–optical relation (SOR) specific to nematic liquids, which we discuss further below.

It is appropriate at this juncture to mention that earlier, using the Erickson polydomain model,⁴⁹ Ugaz and Burghardt⁴⁰ obtained the following expression applicable to steady shear flow of flow-aligning nematics,

$$\frac{N_1}{\sigma} = \frac{2}{\sqrt{\lambda^2 - 1}} \quad (3)$$

where λ is a parameter describing the propensity toward tumbling ($\lambda < 1$) or flow-aligning ($\lambda > 1$) behavior. We note that as the value of λ approaches 1, the closer flow alignment is to the flow direction; i.e., the smaller the angle is between the nematic director and the flow axis.⁵³ Ugaz and Burghardt⁴⁰ also presented a relationship between λ and the local *molecular* order parameter S_m by

$$\lambda = \frac{2 + S_m}{3S_m} \quad (4)$$

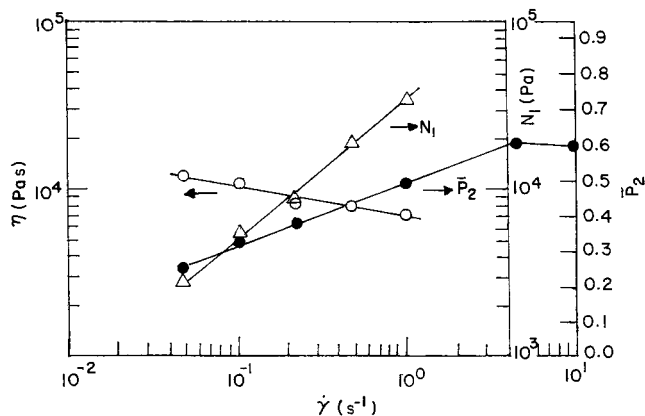


Figure 11. Shear rate dependence of viscosity η (○), first normal stress difference N_1 (Δ), and bulk orientation order parameter \bar{P}_2 (●) in steady-state shear flow of PSHQ10 at 160 °C. \bar{P}_2 was determined from X-ray scattering, which corresponds to the bulk orientation order parameter S defined by eq 5.

in which S_m is related to the bulk orientation parameter S by

$$S = S_m \bar{S} \quad (5)$$

where \bar{S} is the mesoscopic order parameter. Note that S is bulk orientation order parameter usually measured during shearing flow by, for instance, X-ray scattering.^{9,40} In view of the fact that the TLCPs under investigation in this study are semiflexible TLCPs having pendant side groups, eq 4 would describe their molecular orientations only qualitatively *if* those polymers are assumed to be of “flow-aligning” type.

Similarly, assuming that the polymers under investigation in this study are “flow aligning,” and using the values of N_1/σ in the nematic region given in Figure 8, we can estimate λ from eq 3 and S_m from eq 4. Because eq 3 is only applicable for $\lambda > 1$, however, such estimations would never allow discernment of flow aligning versus tumbling behavior. This said, we obtain (i) $\lambda = 1.019$ and $S_m = 0.972$ for PEHQ10 using $N_1/\sigma = 10$, (ii) $\lambda = 1.021$ and $S_m = 0.969$ for PEHQ10 using $N_1/\sigma = 9$, and (iii) $\lambda = 1.031$ and $S_m = 0.956$ for PSHQ10 using $N_1/\sigma = 8$. The values of λ estimated above indicate that the degree of flow alignment for PEHQ10 is higher than that of PTHQ10, and that of PTHQ10 is higher than PSHQ10. Such an observation is in line with the intuitive expectation that the smaller the pendant side groups, the higher the flow alignment will be. We note that, from Table 1, the van der Waals volume of the three pendant side groups has the following increasing order: ethoxy group in PEHQ10 < *tert*-butyl group in PTHQ10 < phenylsulfonyl in PSHQ10. However, the values of S_m estimated above for the three TLCPs are excessively high. The results of our recent X-ray scattering study,⁵⁴ summarized in Figure 11, indicate that for PSHQ10 at 160 °C $S (=S_m \bar{S})$ varies from ca. 0.3 to ca. 0.6 as the shear rate is increased from 0.05 to 5 s⁻¹. Thus, the large values of $S_m = 0.956–0.972$ estimated from eq 4 for the three TLCPs suggest surprisingly low values for \bar{S} (~0.5), in apparent contradiction with experiments for the range of shear rates tested.

4. Concluding Remarks

In this paper we have shown how the size of pendant side groups can strongly affect the flow birefringence.

We found that all three TLCPs investigated show flow-induced alignment, though with weak birefringence oscillations, and that the size of pendant side groups attached to the mesogenic main chain appears to have a subtle influence on the extent of flow alignment; the smaller the size of pendant groups, the greater the alignment in the flow direction.

We have shown flow-induced molecular alignment characteristics of the three TLCPs investigated through the use of spectrographic birefringence and unpolarized transmission measurements as functions of time. We found that (i) variations in spectrum amplitude and unpolarized transmission with time are very similar to that reported previously by Ugaz and Burghardt,⁴⁰ who also employed a semiflexible main-chain TLCP with phenylsulfonyl pendant side groups, (ii) the magnitude and rate of growth in spectrum amplitude, upon startup of shear flow, depend very much on the size of pendant side groups and the molecular weight of TLCPs, and (iii) upon startup of shear flow, those TLCPs with larger pendant side groups feature enhanced textural coarsening compared to those having smaller pendant side groups.

We wish to mention that our experimental data on N_1 are reproducible, and they have not arisen from experimental artifacts. On the basis of the reproducibility in both position and magnitude from one experiment to the next, which temperature fluctuations (to within ± 1 °C) would not satisfactorily explain, we do not attribute the weak N_1 oscillations (and N_1/σ oscillations) observed in this study to temperature fluctuations. Likewise, the weak birefringence oscillations are very reproducible in strain position and magnitude from one experiment to the next, and their appearance suggests an enhanced sensitivity of birefringence over wide-angle X-ray scattering under similar conditions.

At present we are not certain that the appearance of a single, large overshoot in $\sigma^+(t, \dot{\gamma})$ alone, during transient shear flow, is sufficient to determine whether an LCP is "tumbling" or "flow aligning" without examining if the same polymer exhibits negative or positive N_1 . We are of the opinion that $N_1^+(t, \dot{\gamma})$ versus $\dot{\gamma}t$ plots are far more sensitive than $\sigma^+(t, \dot{\gamma})$ versus $\dot{\gamma}t$ plots to the structural response of an LCP. After all, the currently held theory^{47,48} suggests that $N_1^+(t, \dot{\gamma})$ versus $\dot{\gamma}t$ plots be used to determine whether an LCP is flow aligning or tumbling.

We are not aware of any meaningful molecular studies enabling us to predict transient shear flow of semiflexible main-chain TLCPs with or without pendant side groups. We expect the partial flexibility of the segmented TLCP chains would play an important role in determining transient shear flow behavior. To accurately describe the dynamics of semiflexible main-chain TLCPs having bulky pendant side groups and the nematic mesophase of polydomain nature, we need an expression, theoretical or empirical, describing the intermolecular (excluded-volume) potential of such polymers. To the best of our knowledge, such an expression has not been developed yet.

By investigating the effect of shear rate on the flow-induced molecular alignment of the TLCPs investigated, we have additionally found that the flow birefringence of TLCPs having smaller pendant groups was insensitive to shear rate while the flow birefringence of TLCPs having bulky pendant groups increased with increasing shear rate. Finally, we have found a remarkable correlation between birefringence Δn and stress ratio N_1/σ

in the nematic region during steady-state shear flow at low shear rates for all TLCPs investigated.

Acknowledgment. C.D.H. acknowledges that this study was supported in part by the National Science Foundation under Grant CTS-9614929.

References and Notes

- (1) Wale, J. L. S. *Rheol. Acta* **1969**, *8*, 38.
- (2) Wale, J. L. S.; Janeschitz-Kriegl, H. *J. Polym. Sci., Part A-2* **1967**, *5*, 781.
- (3) Adams, J. W. C.; Janeschitz-Kriegl, H.; den Otter, J. L.; Wale, J. L. S. *J. Polym. Sci., Part A-2* **1968**, *6*, 871.
- (4) Funatsu, K.; Mori, Y. *Chem. High Polym. (Jpn.)* **1968**, *25*, 337.
- (5) Han, C. D.; Drexler, L. H. *J. Appl. Polym. Sci.* **1973**, *17*, 2329.
- (6) Han, C. D.; Drexler, L. H. *J. Appl. Polym. Sci.* **1973**, *17*, 2369.
- (7) Hongladarom, K.; Burghardt, W. R. *Macromolecules* **1993**, *26*, 785.
- (8) Hongladarom, K.; Secakusuma, V.; Burghardt, W. R. *J. Rheol.* **1994**, *38*, 1505.
- (9) Hongladarom, K.; Ugaz, V. M.; Cinader, D. K.; Burghardt, W. R.; Quintana, J. P.; Hsiao, B. D.; Dadmun, M. D.; Hamilton, W. A.; Butler, P. D. *Macromolecules* **1996**, *29*, 5346.
- (10) Chen, Z.-R.; Kornfield, J. A.; Smith, S. D.; Grothaus, J. T.; Satkowski, M. M. *Science* **1997**, *277*, 1248.
- (11) Fuller, G. G. *Optical Rheometry of Complex Fluids*; Oxford University Press: New York, 1995.
- (12) Lin, Y. G.; Winter, H. H. *Macromolecules* **1991**, *24*, 2877.
- (13) Kim, S. S.; Han, C. D. *Macromolecules* **1993**, *26*, 3176.
- (14) Kim, S. S.; Han, C. D. *J. Rheol.* **1993**, *37*, 847.
- (15) Han, C. D.; Chang, S.; Kim, S. S. *Mol. Cryst. Liq. Cryst.* **1994**, *254*, 335.
- (16) Gilmore, J. R.; Colby, R. H.; Hall, E.; Ober, C. K. *J. Rheol.* **1994**, *38*, 1623.
- (17) Furukawa, A.; Lenz, R. W. *Macromol. Chem., Macromol. Symp.* **1986**, *2*, 3.
- (18) Lenz, R. W.; Furukawa, A.; Bhowmik, P. K.; Garay, R. O.; Majnusz, J. *Polymer* **1991**, *32*, 1703.
- (19) Kim, S. S.; Han, C. D. *Polymer* **1994**, *35*, 93.
- (20) Chang, S.; Han, C. D. *Macromolecules* **1997**, *30*, 1670.
- (21) Mather, P. T.; Grizzuti, N.; Feffner, G.; Ricker, M.; Rochefort, W. E.; Seitz, M.; Schmidt, H.-W.; Pearson, D. S. *Liq. Cryst.* **1994**, *17*, 811.
- (22) Kim, D.-O.; Han, C. D. *Macromolecules* **2000**, *33*, 3349.
- (23) Mather, P. T.; Stüber, H. R.; Chaffee, K. P.; Haddad, T. S.; Romo-Uribe, A.; Lichtenhan, J. D. In *Liquid Crystals for Advanced Technologies*; Chen, S., Bunning, T., Eds.; MRS Symp. Proc. No. 425; MRS: Washington, DC, 1996; p 137.
- (24) Mather, P. T.; Romo-Uribe, A.; Han, C. D.; Kim, S. S. *Macromolecules* **1997**, *30*, 7977.
- (25) Mather, P. T. Unpublished results, 1997.
- (26) Hongladarom, K.; Burghardt, W. R.; Baek, S. G.; Cementwala, S.; Magda, J. J. *Macromolecules* **1993**, *26*, 772.
- (27) Beekmans, F.; Posthuma de Boer, A. *Macromolecules* **1996**, *29*, 8726.
- (28) Born, M.; Wolf, E. *Principles of Optics*; Pergamon: New York, 1980.
- (29) Mather, P. T.; Jeon, H. G.; Han, C. D.; Chang, S. *Macromolecules*, in press.
- (30) Kim, C. D.; Han, C. D. *Macromolecules* **1993**, *26*, 6, 6633.
- (31) Blumstein, A.; Vilasagar, S.; Ponrathnam, S.; Clough, S. B.; Blumstein, R. B.; Maret, G. *J. Polym. Sci., Polym. Phys. Ed.* **1982**, *20*, 877.
- (32) Majnusz, J.; Catala, J. M.; Lenz, R. W. *Eur. Polym. J.* **1983**, *19*, 1043.
- (33) Blumstein, R. B.; Stickles, E. M.; Gauthier, M. M.; Blumstein, A.; Volino, F. *Macromolecules* **1984**, *17*, 177.
- (34) Percec, V.; Tomazos, D.; Pugh, C. *Macromolecules* **1989**, *22*, 3259.
- (35) Laus, M.; Sante Angeloni, A.; Galli, G.; Chiellini, E. *Macromolecules* **1992**, *25*, 5901.
- (36) Wunder, S. L.; Ramachandran, S.; Cochanour, C. R.; Weinberg, M. *Macromolecules* **1986**, *19*, 1696.
- (37) Irwin, R. S.; Sweeny, W.; Gardner, K. H.; Gochanour, C. R.; Weinberg, M. *Macromolecules* **1989**, *22*, 1065.
- (38) Kim, S. S.; Han, C. D. *J. Polym. Sci., Polym. Phys. Ed.* **1994**, *32*, 371.
- (39) Chang, S.; Han, C. D. *Macromolecules* **1997**, *30*, 2021.

- (40) Ugaz, V. M.; Burghardt, W. R. *Macromolecules* **1998**, *31*, 8474.
- (41) Baek, S. G.; Magda, J.; Larson, R. G.; Hudson, S. D. *J. Rheol.* **1994**, *38*, 1473.
- (42) Chang, S.; Han, C. D. *Macromolecules* **1997**, *30*, 1656.
- (43) Zhou, W. J.; Kornfield, J. A.; Ugaz, V. M.; Burghardt, W. R.; Link, D. R.; Clark, N. A. *Macromolecules* **1999**, *32*, 5581.
- (44) Marrucci, G.; Maffettone, P. L. *J. Rheol.* **1991**, *34*, 1217; 1231.
- (45) Maier, W.; Saupe, A. *Z. Naturforsch.* **1958**, *13A*, 564; **1959**, *14A*, 882; **1960**, *15A*, 287.
- (46) Doi, M. *J. Polym. Sci., Polym. Phys. Ed.* **1981**, *19*, 229.
- (47) Marrucci, G.; Maffettone, P. L. *Macromolecules* **1989**, *22*, 4076.
- (48) Larson, R. L. *Macromolecules* **1990**, *23*, 3983.
- (49) Ericksen, J. L. *Arch. Ration. Mech. Anal.* **1960**, *4*, 231.
- (50) Burghardt, W. R. Personal communication.
- (51) Nakai, A.; Wang, W.; Hashimoto, T.; Blumstein, A.; Maeda, Y. *Macromolecules* **1994**, *27*, 6963.
- (52) Nakai, A.; Wang, W.; Hashimoto, T.; Blumstein, A. *Macromolecules* **1996**, *29*, 5288.
- (53) Mather, P. T.; Pearson, D. S.; Burghardt, W. R. *J. Rheol.* **1995**, *39*, 627.
- (54) Mather, P. T.; Han, C. D. Unpublished research, 1998.

MA000750T